THE JOURNAL OF PHYSICAL CHEMISTRY C

Article

Cite This: J. Phys. Chem. C 2017, 121, 22700-22706

pubs.acs.org/JPCC

Anisotropic Electric Field Effect on the Photoluminescence of $CH_3NH_3PbI_3$ Perovskite Sandwiched between Conducting and Insulating Films

Kamlesh Awasthi, Chi-Yung Wang, Amir Fathi, Sudhakar Narra, Eric Wei-Guang Diau,* and Nobuhiro Ohta*

Department of Applied Chemistry and Institute of Molecular Science, National Chiao Tung University, Hsinchu 30010, Taiwan

Supporting Information

ABSTRACT: Photoluminescence (PL) of a nanocrystalline film of methylammonium lead iodide perovskite ($MAPbI_3$) sandwiched between an electrode of a fluorine-doped tin oxide (FTO) layer and an insulating film of poly(methyl methacrylate) is found to increase and decrease significantly with the application of an external electric field (F_{ext}), depending on the direction of the applied field, based on the measurements of electrophotoluminescence (E-PL) spectra, i.e., field-induced change in PL spectra. The field-induced change in PL intensity is confirmed to originate from the field-induced change in the number of free carriers which induce radiative recombination, based on temporally resolved E-PL measurements. We propose that an internal field (F_{int}) exists even without application of F_{ext}. The anisotropic behavior of the effect of F_{ext} on PL is interpreted in terms of a synergy effect of F_{int} and F_{ext}; both fields are additive with the applied field direction from Ag to FTO electrode (positive direction) or subtractive with the opposite applied field direction (negative direction), where FTO is the positive electrode, resulting in an increased or decreased total electric field as well as quenching or enhancement of PL, respectively. The PL lifetime in the nanosecond region increased and decreased with an application of an electric field in the positive and negative directions, respectively, which is attributed to a field-induced change in the concentration of free carriers.

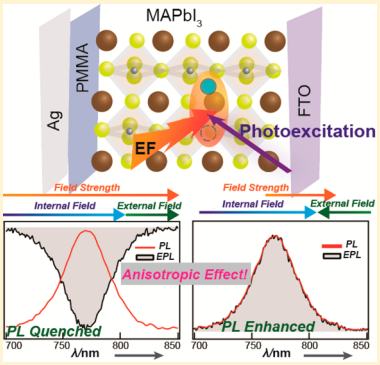

1. INTRODUCTION

Understanding photogenerated carriers and excitons in an organic−inorganic hybrid perovskite is one of the most attractive subjects in the fields of optics, spectroscopy, and material sciences, because of the prospective applications of these materials in optoelectronic and photonic devices such as solar cells, light-emitting diodes, photodetectors, lasers, and field-effect transistors.[1−5] The application of perovskite materials in photovoltaic devices has increased the power conversion efficiency over ∼22% in a short period,[6−8] as a result of a large carrier diffusion length,[9,10] ambipolar carrier conduction,[11] small exciton binding energy, and small rate of charge recombination.[12,13]

To elucidate the working mechanism of perovskite-based optoelectronic and photonic devices, which might translate into improved device performances, many studies such as of photoluminescence, temporally resolved microwave conductivity, and transient absorption have been conducted to reveal the nature of charge carriers created in these materials and their kinetic behavior, but the nature of photoexcitation across the band gap remains a subject for debate and research.[9,10,14−19]

Two distinct mechanisms of carrier generation in photovoltaic cells following photoexcitation can be considered: a free-carrier model and an exciton model. In the former case, the recombinations of free electrons and holes are dominant processes in photoexcited states, whereas free electrons and holes are produced in the latter through dissociation of an exciton (electron−hole pair) that has some binding energy. In organic photovoltaic cells, exciton generation by photoexcitation, migration, and dissociation to produce free electron and hole are the main processes; carriers are generally considered to be produced through excitons.[20,21] In contrast with organic solar cells, the consensus is that free carriers are dominant in hybrid lead halide perovskites.[17,19,22−24] The carrier-generation mechanism seems hence to differ between organic solar cells and cells constructed with lead halide perovskites.

An electric field has been extensively used to modulate the level structure and dynamics of the excited state including charge transfer.[25] It was shown that the measurements of electrophotoluminescence (E-PL) spectra, i.e., the electric-field-induced change in photoluminescence (PL) spectra, were useful to illuminate the working mechanism in organic dye-sensitized solar cells (DSSCs). The field-induced quenching of PL is well correlated in organic photovoltaic cells with the performance of photovoltaic cells.[26,27] If the carrier generation mechanism differs between organic sensitizers and organo lead halide perovskites, it is of interest to ascertain the difference in

Received: August 8, 2017
Revised: September 21, 2017
Published: September 26, 2017

DOI: 10.1021/acs.jpcc.7b07883
J. Phys. Chem. C 2017, 121, 22700−22706

the effects of an electric field on the PL property between these materials.

Electron−hole interaction and carrier recombination, which are essential for the efficient functioning of these materials in photovoltaic devices, were recently shown to be modulated with an electric field through the reorientation and movement of molecular dipoles. In a solid film of methylammonium lead triiodide ($MAPbI_3$) sandwiched between two noninjected Al_2O_3 layers, for example, an electron−hole interaction as well as the photogenerated carrier dynamics was shown to be affected by an applied electric field, based on the steady-state and time-resolved PL measurements, when such a field was applied.[28] A field-induced carrier drift that induces PL quenching and field-induced defect migration were suggested to occur in $MAPbI_3$ near 300 K. At 190 K, dipole alignment and structural ordering induced by an electric field, which results in enhanced electron−hole interaction and increased rate of radiative decay, was suggested. The influence of ion conformational and translational dynamics on charge dynamics has been also examined following photoexcitation in methylammonium lead tribromide ($MAPbBr_3$) under an applied electric field, based on the temporally resolved PL measurements over time scales from ∼100 ps to 10 s. PL modulation was then observed over a range of time scale ∼ 100 ps to 100 ms, which was attributed mainly to field-induced reorientation of a molecular cation group.[29] The field effect on PL observed in lead halide perovskites seems hence to differ greatly from that observed in dye-sensitized solar cells.

In the experiments on effects of electric field in PL reported so far, organo lead halide perovskites were sandwiched between noninjecting contacts. For example, a $MAPbI_3$ film was sandwiched between Al_2O_3 films or $MAPbBr_3$ crystals were dispersed into a polystyrene (PS) host matrix sandwiched between SiO_2 and aluminum.[28,29] The temporally resolved PL decays at both positive and negative biases were there the same, and PL components showed no apparent dependence on the direction of the applied electric field. In organo lead trihalide perovskite-based photovoltaic devices, in contrast, a field-switchable photovoltaic effect was observed;[30] that is, the photocurrent direction was switched on application of a small electric field with the opposite direction, likely resulting from a switchable field-induced ion drift in the perovskite layer. In the present work, we measured E-PL spectra and field-induced change in temporally resolved PL decay for a $MAPbI_3$ nanocrystalline film sandwiched between conducting and insulating films, i.e., between a fluorine-doped tin oxide (FTO) electrode and a poly(methyl methacrylate) (PMMA) insulator film. We devoted particular attention to the field direction dependence of the field effects on photoexcitation dynamics. An anisotropic behavior of the effects of electric field on the PL of $MAPbI_3$ films has been clearly observed, such that field-induced quenching and enhancement of PL depended on the direction of an applied electric field. The present results indicate that a population of the free carriers that show the radiative recombination of electron and hole pairs to be enhanced and suppressed on application of an electric field in a $MAPbI_3$ nanocrystalline film, respectively, depending on the field direction. We observed further a field-induced increase and decrease of the PL lifetime in the nanosecond range that depended on the field direction, indicating that radiative bimolecular processes of free electrons and holes in a thermalized state are also affected by an electric field. These anisotropic field effects on PL might yield guidance in considering the operating mechanism of optoelectronic devices with perovskite materials, including the hysteresis behavior observed in voltage−current plots in photovoltaic devices.

2. EXPERIMENTAL SECTION

The $MAPbI_3$ thin film was prepared on a $TiCl_4$-treated FTO-coated glass substrate on the spin-coating for 30 s of a perovskite solution (45 mass %, which includes PbI_2 (578 mg) and MAI (200 mg) of DMF (1 mL)). After a delay of 4 s, chlorobenzene (240 μL) was quickly added onto the spinning film to obtain homogeneous perovskite film of smaller size and thickness ∼ 270 nm; an insulating layer of PMMA film was then deposited on the perovskite thin film. The total thickness of perovskite and PMMA films was determined by the SEM image measurements to be ∼1 μm or less. One example of the SEM images both of $MAPbI_3$ crystals and of the layer structure of the FTO/$MAPbI_3$/PMMA is shown in Figure 1. The

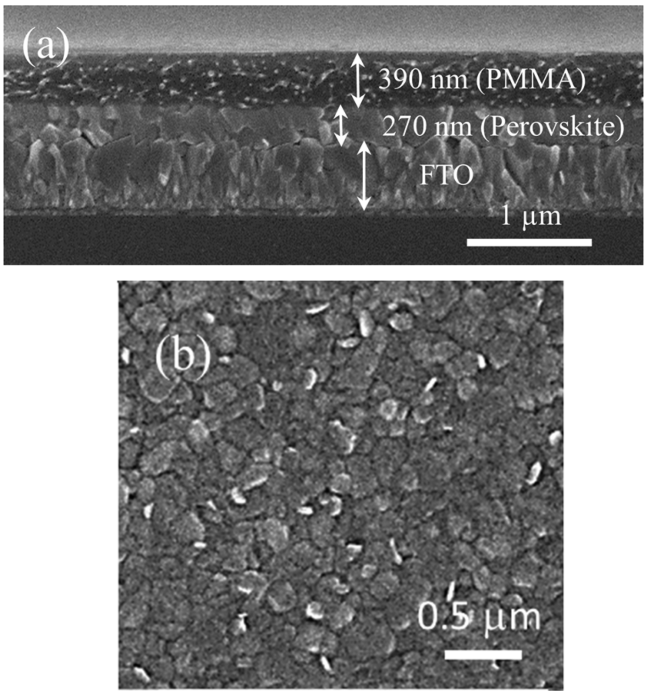

Figure 1. (a) SEM image of the layer structure of FTO/$MAPbI_3$/PMMA coated on the glass plate and (b) SEM image of prepared $MAPbI_3$ crystals.

thickness of $MAPbI_3$ films was also estimated by comparing the absorption intensity of the exciton band at 750 nm. A semitransparent Ag film of thickness ∼ 25 nm was further deposited on the PMMA film through thermal deposition. FTO and Ag films served as electrodes for the E-PL measurements. A schematic illustration of the sandwich film of perovskite is shown in Figure 2.

Steady-state E-PL spectra were recorded with modulated electric field by using a spectrometer (Jasco FP777) combined with a lock-in amplifier.[31] Excitation light at 450 nm which propagates in the plane including the normal direction of the sample plate was incident to the electrode with the angle larger than 45° between the propagation direction of the excitation light and the normal direction of the sample. The sample was arranged to minimize the scattered light which entered to the monochromator for detection, i.e., PL transmitted through both $MAPbI_3$ layer and another electrode, which is different from the

DOI: 10.1021/acs.jpcc.7b07883
J. Phys. Chem. C 2017, 121, 22700−22706

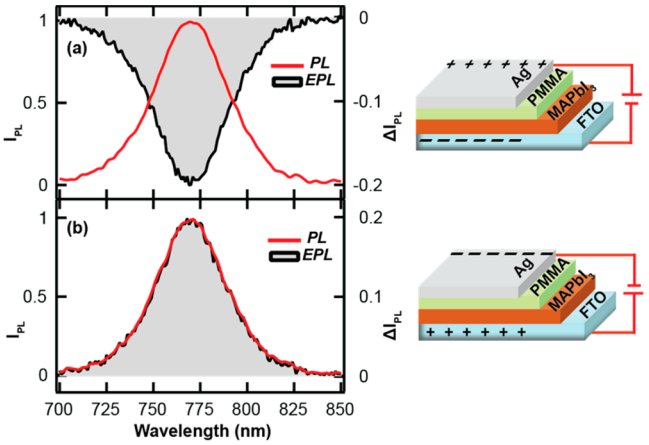

Figure 2. Schematic illustration of the sandwich films of $MAPbI_3$ perovskite with respect to the directions of applied electric field, and PL (red line) and E-PL spectra (shaded line) of perovskite thin film with a field strength of 0.3 MV cm^{-1}. In (a), the direction of the external electric field is toward the FTO electrode from the Ag electrode (positive direction), and in (b), the direction of the external electric field is toward the Ag electrode from the FTO electrode (negative direction).

one facing the incoming excitation light, was dispersed by the monochromator and detected by the photomultiplier. Details of the experimental procedures appear in the Supporting Information. The PL intensity and its field-induced change, i.e., I_{PL} and ΔI_{PL}, respectively, were measured together. The field strength was determined from the applied voltage divided by the distance between FTO and Ag films. In the PL decay measurements, the second harmonic of the laser light (450 nm) of a mode-locked Ti:sapphire laser (Spectra Physics, Tsunami, pulse width ~ 100 fs) served for excitation; the PL was detected with a microchannel plate photomultiplier (Hamamatsu, R3809U) in a single-photon-counting system.[32] Regarding the position relation between the incident laser light and the sample plate, the arrangement which was essentially the same as the one used for the steady-state E-PL measurements was used, and PL transmitted through the $MAPbI_3$ layer was detected. Details of the decay measurements are shown in the Supporting Information and Figure S1.

3. RESULTS AND DISCUSSION

E-PL spectra of $MAPbI_3$ film were recorded at the first harmonic of the modulation frequency with field strength 0.3 MV cm^{-1}. For excitation at 450 nm, the field-induced change in absorption intensity was negligible. The results are shown in Figure 2, together with the PL spectra. Here and hereafter, the direction of the electric field applied to a $MAPbI_3$ film shown in Figure 2a, in which FTO is the negative electrode, is denoted as the positive direction, whereas the opposite direction, shown in Figure 2b, is regarded as the negative direction. The E-PL spectra show that the intensity, i.e., the quantum yield of PL, decreases and increases, respectively, on application of an electric field in the positive direction (Figure 2a) and in the negative direction (Figure 2b). The magnitude of the field-induced change in PL intensity (ΔI_{PL}) relative to the PL intensity at zero field (I_{PL}) is linearly proportional to the strength of the applied field, as shown in Figure 3; the magnitude of $\Delta I_{PL}/I_{PL}$ was as large as ~20% at field strength 0.3 MV cm^{-1}. It is noted that the results shown in Figure 2 were obtained with the experimental condition where the Ag

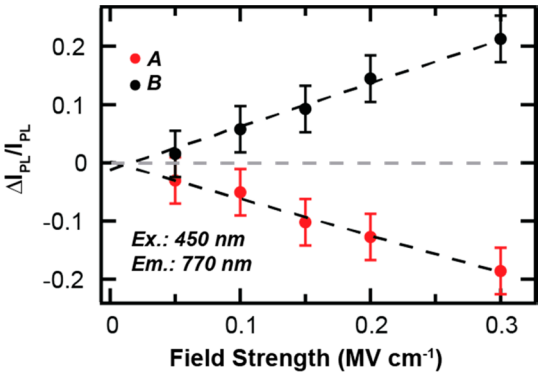

Figure 3. Electric field strength dependence of the field-induced change in PL intensity. Plots of $\Delta I_{PL}/I_{PL}$ as a function of applied electric field strength. A and B correspond to the applied electric field having positive and negative applied field directions, respectively (see Figure 2).

electrode was facing the 450 nm excitation light and that the PL transmitted through the $MAPbI_3$ layer and FTO layer was detected. It was confirmed that the results were essentially the same, even when the PL measurements were done with the FTO layer facing the incident excitation light. E-PL spectra were also recorded at the second harmonic of the modulation frequency of the applied electric field. As shown in Figure S2 of the Supporting Information, ΔI_{PL} obtained at the second harmonic of the modulation frequency was positive, indicating the field-induced increase of the quadratic term of the PL intensity, but the magnitude of $\Delta I_{PL}/I_{PL}$ was as small as about 5×10^{-4} at field strength 0.3 MV cm^{-1}.

According to the consensus, the PL of a $MAPbI_3$ film is emitted as a result of a radiative carrier recombination. As shown in Figure S3 of the Supporting Information, the lifetime of the rapid decay of the PL has been confirmed to be 175 fs with excitation at 450 nm, indicating that the PL of $MAPbI_3$ observed at 670 nm is emitted from hot carriers produced by photoirradiation.[16] In contrast with the PL at 670 nm, the strong PL that shows a maximum intensity at 770 nm is considered to be emitted by radiative recombination of thermalized free carriers, not hot carriers. These PL emissions are hereafter called as hot PL and cold PL, respectively. The PL spectra shown in Figure 2 correspond predominantly to the cold PL.

As the processes following photoexcitation, which decay with the average lifetime of 175 fs, the next processes are considered: (1) radiative geminate recombination of photogenerated hole−electron pairs, which produce the hot PL; (2) quick thermalization of hot carriers to the extremes of conduction and valence bands, that is, a relaxation of photogenerated hot carriers to the conduction state of least energy and highest valence state, respectively, which results in intense PL with a maximum at 770 nm by a radiative recombination; (3) drift of hot carriers following dissociation of photogenerated hole−electron pairs, which is a nonradiative dissociation of photogenerated electron−hole pairs. In the present experiments, the intensity of irradiation light was not strong; the nonradiative electron−hole annihilation via Auger processes can be excluded.[16] The present results then imply that the population of the emitting state of the cold PL, that is, the number of free carriers that produce the cold PL, might be decreased or increased on application of an electric field, depending on the direction of that applied field. As mentioned

DOI: 10.1021/acs.jpcc.7b07883
J. Phys. Chem. C 2017, 121, 22700−22706

above, such free carriers are produced by relaxation of photogenerated hot carriers, in competition both with radiative geminate recombination of photogenerated electron−hole pairs and with nonradiative drift of dissociated hot electrons and holes. As a mechanism of the quenching and the enhancement of PL in the presence of an electric field, another possibility is that the field effect results from an altered rate of a radiative process or a nonradiative process at the emitting state of the cold PL. To distinguish these two mechanisms, we measured PL decay profiles of $MAPbI_3$ on monitoring the PL at 770 nm at zero field and in the presence of an electric field (0.3 MV cm^{-1}). The results appear in Figure 4, together with the ratio

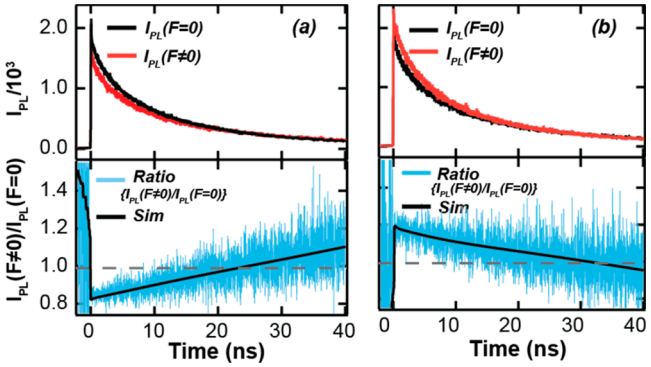

Figure 4. PL decay profiles observed with and without application of electric field. PL decay of a $MAPbI_3$ thin film at 770 nm in the absence (black line) and in the presence of 0.3 MV cm^{-1} (red line). In part (a), the applied electric field was directed from the Ag to the FTO electrode (positive direction), and in (b), the applied electric field was directed from the FTO to the Ag electrode (negative direction). The ratio of the decay profile observed at 0.3 MV cm^{-1} relative to that at zero field (red line) together with a simulated one (black line) is shown at the bottom of (a) and (b), respectively. These results were obtained with laser fluence ∼ 0.1 μJ cm^{-2} (excitation density ∼ 5 × 10^{16} cm^{-3}) at 450 nm.

between two decays observed with and without electric field, i.e., $I_{PL(F\neq0)}/I_{PL(F=0)}$. The observed PL shows a nonexponential decay, likely because the PL lifetimes vary between grains.[33,34] The observed decay profiles were simulated on assuming a triexponential decay, i.e., $\Sigma_i A_i \exp(-t/\tau_i)$, in which A_i and τ_i represent pre-exponentail factor and emission lifetime of component i, respectively. The lifetime and pre-exponential factor of each component simulated for the observed decay are shown in Table 1.

As shown in Figure 4 and Table 1, the ratio of $I_{PL(F\neq0)}/I_{PL(F=0)}$ at time $t = 0$ was less than unity in the positive direction, but larger than unity in the negative direction. These results indicate that the population of the free carriers that produce the cold PL with a maximum at 770 nm decreases and increases on application of an electric field in the positive and negative directions, respectively. The yield of the accumulation of electrons and holes at the bottom and top of the conduction and valence bands is hence not unity. Note that the accumulation competes both with the radiative geminate recombination that produces hot PL and with the nonradiative drift of generated hot carriers following photoexcitation. The anisotropic field-induced change in quantum yield of PL is then ascribed to the field effect on the population of the emitting state of the cold PL; that is, the number of free carriers for the cold PL is influenced with an applied electric field. The temporal dependence of the field-induced change in the rapidly decaying component in the sub-picosecond region was undetectable in the present experiments because of the limited time resolution in the measurements of the field effects on decay profile, but the results shown in Figure 4 imply that the rapid processes that occur in the sub-picosecond region are affected by applied electric fields.

As the origin of the field-induced change in population of the emitting state of the cold PL, a field-induced drift of photocarriers to the electrode can be considered; photogenerated electrons and holes drift to opposite sides of electrodes in the presence of an electric field, diminishing the probability of their recombination. An anisotropic behavior, i.e., the dependence of the PL intensity and the decay profile on the field direction, might be interpreted in terms of a synergistic effect of externally applied electric field ($\boldsymbol{F}_{ext}$) and internal field ($\boldsymbol{F}_{int}$) produced in the $MAPbI_3$ film sandwiched between the electrode of FTO and insulating film of PMMA.

The electroconductivity of the present $MAPbI_3$ film can be regarded as n-type, for which the electron concentration is large, because the perovskite was grown under conditions that the ratio of lead iodide (PbI_2) to methylammnonium iodide (MAI) in the precursor mixture solution was 1.0.[35] In the $MAPbI_3$ film in contact with a conducting FTO film, therefore, free electrons originally generated in $MAPbI_3$ and generated through dissociation of photoexcited electron−hole pairs might accumulate near an FTO surface even without an application of an electric field, because the Fermi level of FTO (−4.4 eV) is located below the conduction band of $MAPbI_3$ at −3.75 eV.[36] In the results, a local field of which the direction is the same as the positive direction exists in $MAPbI_3$ film even without application of an external electric field. The internal field, $\boldsymbol{F}_{int}$, may be estimated to be 0.7 MV cm^{-1} as a maximum, as shown in the Supporting Information and Figure S4. The optical transition of PMMA is located in the UV region, and the LUMO and HOMO levels are located at −1.8 and −7.3 eV, respectively.[37] As mentioned above, the $MAPbI_3$ layer is regarded as the electron-rich materials, but the PMMA layer is regarded as a charge blocking layer because the LUMO level of PMMA is located much higher than the conduction state of $MAPbI_3$. In the results, the internal field induced by interaction between $MAPbI_3$ and PMMA is not necessary to be considered, in contrast with the interface between FTO and $MAPbI_3$. Under such conditions, the total electric field is enhanced with

Table 1. Lifetime (τ_i) and Pre-exponential Factor (A_i, in Parentheses) of Each Decaying Component of PL Observed at Zero Field and at 0.3 MV cm^{-1} (in the Positive and Negative Directions), Where $\Sigma_{i=1}^{3} A_i$ Was Normalized To Be Unity at Zero Field. The Average Lifetime and a Sum of the Pre-exponential Factors in Each Decay Profile Are Also Shown

	τ_1 (ns) (A_1)	τ_2 (ns) (A_2)	τ_3 (ns) (A_3)	τ_{avg} (ns) ($\Sigma_{i=1}^{3} A_i$)
$\boldsymbol{F}$ (0)	0.10 (0.609)	6.20 (0.231)	24.02 (0.160)	5.34 (1.0)
$\boldsymbol{F}$ (+0.3 MV cm^{-1})	0.10 (0.495)	6.46 (0.185)	27.61 (0.137)	6.16 (0.817)
$\boldsymbol{F}$ (−0.3 MV cm^{-1})	0.10 (0.722)	5.83 (0.273)	21.42 (0.191)	4.85 (1.186)

DOI: 10.1021/acs.jpcc.7b07883
J. Phys. Chem. C 2017, 121, 22700−22706

an external electric field, F_{ext}, applied in the positive direction, whereas the total field strength decreases, when F_{ext} is applied in the negative direction (see Figure 5), because the directions

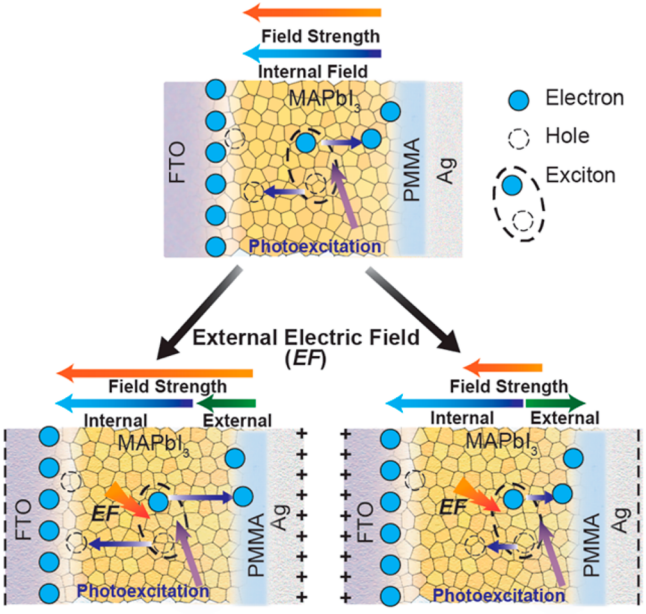

Figure 5. Schematic illustration of the total electric fields before and after application of an external electric field. Applied electric field and internal field are additive (left) and subtractive (right), respectively.

of F_{int} and F_{ext} are opposite to each other in the negative direction. In the presence of F_{int}, photogenerated hot electrons and holes are considered to move to opposite sides of electrodes, which decreases both the probability of radiation recombination and the population of free carriers for the cold PL. In the results, cold PL is considered to be decreased by the internal field. When F_{ext} is applied in the positive direction, the total field strength increases; the drift of hot electrons and holes becomes more efficient, resulting in an enhanced PL quenching. When F_{ext} is applied in the negative direction, the strength of the total field applied to the sample decreases relative to the strength of F_{int} (see Figure 5). The quenching induced by the internal field is then recovered, resulting in an enhanced cold PL on application of F_{ext} in the negative direction. The anisotropic behavior of field-induced change is thus interpreted on considering that the total electric field in $MAPbI_3$ is increased and decreased on application of F_{ext}, respectively, in the positive and negative directions.

In addition to the field-induced change in the population of free carriers for the cold PL, another field effect is perceptible in the decay measurements. As Figure 4 shows, the ratio $I_{PL(F\neq 0)}/I_{PL(F=0)}$ increases and decreases monotonically as a function of passage of time in the positive and negative directions, respectively. These results show that the lifetime of PL in the nanosecond range is altered on application of F_{ext}. The lifetime of each decay component increases with F_{ext} in the positive direction, but decreases with F_{ext} in the negative direction (see Table 1). There is no doubt that the rate of nonradiative decay of free carriers in the thermalized state, which competes with the radiative bimolecular recombination, decreases and increases on application of F_{ext} in the positive and negative directions, respectively.

In the thermalized conduction state, trapping of electros to a defect or surface state might be efficient, in competition with the radiative recombination between electrons and holes. Trapped electrons might recombine nonradiatively with holes in the valence bands at later times.[38] As mentioned already, the population of the free carriers that produce the cold PL is affected by an application of F_{ext}. The field-induced variation in the number of free carriers might produce a change in the number of trapped electrons; the decreased number of free carriers on application of F_{ext} in the positive direction might decrease the number of trapped electrons because of the small carrier density, whereas the number of trapped electrons might increase on application of F_{ext} in the negative direction. The decreased and increased number of trapped electrons might result in the decreased and increased rate of nonradiative recombination as well as the increased and decreased PL lifetime, respectively, with application of F_{ext} in the positive and negative directions.

The earlier reports of the effects of electric field on PL intensity and on lifetime of $MAPbI_3$ sandwiched between two noninjecting Al_2O_3 layers highlight the field-induced enduring decrease of PL intensity near 300 K and increase at 190 K.[28] However, the electric field effects on PL of $MAPbI_3$ sandwiched between conducting (FTO) and insulating (PMMA) films are decisively different from the ones reported for $MAPbI_3$ sandwiched between insulating films. In the present results, both the field-induced quenching and the enhancement of PL of $MAPbI_3$ were observed at the same temperature (~297 K) following photoexcitation, simply on altering the direction of the applied field. An enduring nature of the effect of electric field on PL was not confirmed in the present experiments; the photoexcitation dynamics were almost recovered in a short period on removing the applied electric field. As shown in Figure S5 of the Supporting Information, decay profiles in one set of measurements were almost completely recovered, within ±2%, at 5 ms after removing the electric fields for both directions. Note that the observation of the field-induced change was reported even after an electric field was removed both near 300 K and at 190 K in $MAPbI_3$ sandwiched between noninjecting layers.[28] The application of electric fields for a long period might induce a metastable configuration, resulting from the enduring field-induced molecular orientation.[39]

The field-induced dipole alignment and structural ordering induced with an applied electric field and the presence of mobile ions have been suggested to play an important role in the effects of an electric field on the photoexcitaiotn dynamics of $MAPbI_3$. The rotation of CH_3 or NH_3 groups around the C−N axis of the MA^+ ions and also the rotational realignment of the C−N axis within the cage formed between the PbI_3 octahedra of the surrounding lattice have been reported.[40] An electric-field-induced degradation was reported to have occurred in $MAPbI_3$ perovskite solar cells through the field-induced migrations of loosely bound I^- anions and $CH_3NH_3^+$ cations in response to a field direction, which is expected to produce PbI_2.[41,42] In the present work, a field-induced degradation of $MAPbI_3$ films was not confirmed for the field-induced change in PL intensity and PL decay profiles measured near 300 K with a field of strength 0.3 MV cm^{-1} modulated with a frequency less than 50 Hz. We found no evidence for molecular alignment or structural ordering in the presence of an electric field, although these phenomena seem to be common in $MAPbI_3$ sandwiched between an electrode and an insulating film and between noninjecting layers. The aniso-

DOI: 10.1021/acs.jpcc.7b07883
J. Phys. Chem. C 2017, 121, 22700−22706

tropic behavior of the effects of an electric field on PL, which indicates the presence of a large internal electric field, and the quick recovery of the PL property on removing the applied electric field seem to come from the motion of free carriers, i.e., electrons and holes, not ions.

The effects of an electric field on the PL of $MAPbI_3$ observed with F_{ext} in the negative direction resemble those observed for the PL at 190 K,[28] that is, an enhanced initial intensity and a decreased lifetime. As a mechanism of the initial enhancement, an explanation was that electrons and holes undergo geminate recombination, due to the field-induced enhancement of the interaction between electron and hole, resulting in the efficient PL, although the predominant route of PL is regarded as a bimolecular recombination of free carriers. If the geminate recombination were enhanced with an applied electric field, it seems that enhancement should be observed for the hot PL, not for the cold PL. In the present results, it is hence unlikely that the field-induced enhanced cold PL in the negative direction results from an enhanced radiative geminate recombination of hole−electron pairs. On the basis of the present results, the effects of an electric field on PL at low temperatures cannot be discussed satisfactorily; not only the free-carrier model but also the exciton model might, however, have to be considered, in contrast with $MAPbI_3$ near 300 K.

The dependence of photoexcitation dynamics on direction of the applied electric field might be related to the hysteresis observed in the current−voltage plots; the present results might contribute to improve photovoltaic cells using perovskites for efficient conversion of solar energy.

4. CONCLUSION

Photoluminescence (PL) intensity of a nanocrystalline film of $MAPbI_3$ sandwiched between FTO layer and insulating film of PMMA decreases, when the external electric field is applied with the direction toward the FTO electrode (positive direction). On the other hand, PL intensity of $MAPbI_3$ increases, when the external electric field is applied with the opposite direction (negative direction). The field-induced change in PL intensity is confirmed to originate mainly from the field-induced change in the number of free carriers which induce radiative recombination, based on the time-resolved E-PL measurements. It is proposed that an internal field (F_{int}) exists even without application of F_{ext}. The anisotropic behavior of the effect of F_{ext} on PL is interpreted in terms of a synergy effect of F_{int} and F_{ext}; i.e., both fields are additive with the applied field in the positive direction and subtractive with the applied field in the negative direction. In the results, PL intensity decreases and increases, respectively, when the electric field is applied in the positive and negative directions, respectively. The PL lifetime in the nanosecond region was also found to increase and decrease, respectively, when the external electric field was applied in the positive and negative directions. The present findings about the electric-field-induced variation of the PL intensity of a perovskite thin film might have important implications for optoelectronic devices.

■ ASSOCIATED CONTENT

Supporting Information

The Supporting Information is available free of charge on the ACS Publications website at DOI: 10.1021/acs.jpcc.7b07883.

Details of the experimental procedures, second harmonic E-PL spectrum, femtosecond PL decay profile, estimation of internal electric field, endurance effects of electric field on PL decay (PDF)

■ AUTHOR INFORMATION

Corresponding Authors

*E-mail: nohta@nctu.edu.tw (N.O.).
*E-mail: diau@mail.nctu.edu.tw (E.W.-G.D.).

ORCID

Eric Wei-Guang Diau: 0000-0001-6113-5679
Nobuhiro Ohta: 0000-0003-4255-6448

Notes

The authors declare no competing financial interest.

■ ACKNOWLEDGMENTS

N.O. thanks Professor Yuan-Pern Lee for generous support. The Center for Interdisiplinary Science of NCTU and the Ministry of Science and Technology of Taiwan (MOST 105-2113-M-009-003; MOST 105-2119-M-009-011-MY3) provided financial support of this research.

■ REFERENCES

(1) Yu, J. C.; Kim, D. B.; Baek, G.; Lee, B. R.; Jung, E. D.; Lee, S.; Chu, J. H.; Lee, D.-K.; Choi, K. J.; Cho, S.; Song, M. H. High-Performance Planer Perovskite Optoelectronic Devices: A Morphological and Interfacial Control by Polar Solvent Treatment. *Adv. Mater.* **2015**, *27*, 3492−3500.

(2) Tan, Z.-K.; Moghaddam, R. S.; Lai, M. L.; Docampo, P.; Higler, R.; Deschler, F.; Price, M.; Sadhanala, A.; Pazos, L. M.; Credgington, D.; Hanusch, F.; Bein, T.; Snaith, H. J.; Friend, R. H. Bright Light-Emitting Diodes Based on Organometal Halide Perovskite. *Nat. Nanotechnol.* **2014**, *9*, 687−692.

(3) Li, G.; Tan, Z.-K.; Di, D.; Lai, M. L.; Jiang, L.; Lim, J. H-W.; Friend, R. H.; Greenham, N. C. Efficient Light-Emitting Diodes Based on Nanocrystalline Perovskite in a Dielectric Polymer Matrix. *Nano Lett.* **2015**, *15*, 2640−2644.

(4) Liu, J.; Xue, Y.; Wang, Z.; Xu, Z.-Q.; Zheng, C.; Weber, B.; Song, J.; Wang, Y.; Lu, Y.; Zhang, Y.; Bao, Q. Two-Dimensional $CH_3NH_3PbI_3$ Perovskite: Synthesis and Optoelectronic Application. *ACS Nano* **2016**, *10*, 3536−3542.

(5) Lee, M. M.; Teuscher, J.; Miyasaka, T.; Murakami, T. N.; Snaith, H. J. Efficient Hybrid Solar Cells Based on Meso-Superstructure Organometal Halide Perovskites. *Science* **2012**, *338*, 643−647.

(6) Kojima, A.; Teshima, K.; Shirai, Y.; Miyasaka, T. Organometal Halide Perovskites as Visible-Light Sensitizers for Photovoltaic Cells. *J. Am. Chem. Soc.* **2009**, *131*, 6050−6051.

(7) Saliba, M.; Matsui, T.; Seo, J.-Y.; Domanski, K.; Correa-Baena, J.-P.; Nazeeruddin, M. K.; Zakeeruddin, S. M.; Tress, W.; Abate, A.; Hagfeldt, A.; Grätzel, M. Cesium-Containing Triple Cation Perovskite Solar Cells: Improved Stability, Reproducibility and High efficiency. *Energy Environ. Sci.* **2016**, *9*, 1989−1997.

(8) Green, M. A.; Emery, K.; Hishikawa, Y.; Warta, W.; Dunlop, E. D. Solar Cell Efficiency Tables. *Prog. Photovoltaics* **2016**, *24*, 905−913.

(9) Xing, G.; Mathews, N.; Sun, S.; Lim, S. S.; Lam, Y. M.; Grätzel, M.; Mhaisalkar, S.; Sum, T. C. Long-Range Balanced Electron and Hole Transport Lengths in Organic-Inorganic $CH_3NH_3PbI_3$. *Science* **2013**, *342*, 344−347.

(10) Stranks, S. D.; Eperon, G. E.; Grancini, G.; Menelaou, C.; Alcocer, M. J. P.; Leijtens, T.; Herz, L. M.; Petrozza, A.; Snaith, H. J. Electron-Hole diffusion Lengths Exceeding 1 Micrometer in an Organometal Trihalide Perovskite Absorber. *Science* **2013**, *342*, 341−344.

(11) Li, F.; Ma, C.; Wang, H.; Hu, W.; Yu, W.; Sheikh, A. D.; Wu, T. Ambipolar Solution-Processed Hybrid Perovskite Phototransistors. *Nat. Commun.* **2015**, *6*, 8238.

(12) Even, J.; Pedesseau, L.; Katan, C. Analysis of Multivalley and Multibandgap Absorption and Enhancement of Free Carries Related

DOI: 10.1021/acs.jpcc.7b07883
J. Phys. Chem. C 2017, 121, 22700−22706

to Exciton Screening in Hybrid Perovskites. *J. Phys. Chem. C* **2014**, *118*, 11566−11572.
(13) Wehrenfennig, C.; Eperon, G. E.; Johnston, M. B.; Snaith, H. J.; Herz, L. M. High Charge Carrier Mobilities and Lifetimes in Organolead Trihalide Perovskites. *Adv. Mater.* **2014**, *26*, 1584−1589.
(14) Manser, J. S.; Kamat, P. V. Band Filling with Free Charge Carriers in Organometal Halid Perovskites. *Nat. Photonics* **2014**, *8*, 737−743.
(15) Marchioro, A.; Teuscher, J.; Friedrich, D.; Kunst, M.; van de Krol, R.; Moehl, T.; Grätzel, M.; Moser, J.-E. Unravelling the Mechanism of Photoinduced Charge Transfer Processes in Lead Iodide Perovskite Solar Cells. *Nat. Photonics* **2014**, *8*, 250−255.
(16) Hsu, H.-Y.; Wang, C.-Y.; Fathi, A.; Shiu, J.-W.; Chung, C. C.; Shen, P.-S.; Guo, T.-F.; Chen, P.; Lee, Y.-P.; Diau, E. W.-G. Femtosecond Excitonic Relaxation Dynamics of Perovskite on Mesoporous Films of Al_2O_3 and NiO Nanoparticles. *Angew. Chem., Int. Ed.* **2014**, *53*, 9339−9342.
(17) D'Innocenzo, V.; Grancini, G.; Alcocer, M. J. P.; Kandada, A. R. S.; Stranks, S. D.; Lee, M. M.; Lanzani, G.; Snaith, H. J.; Petrozza, A. Excitons versus Free Charges in Organo-Lead Tri-Halide Perovskites. *Nat. Commun.* **2014**, *5*, 3586.
(18) Hutter, E. M.; Eperon, G. E.; Stranks, S. D.; Savenije, T. J. Charge Carrier in Planar and Meso-Structured Organic-Inorganic Perovskites: Mobilities, Lifetimes, and Concentrations of Trap States. *J. Phys. Chem. Lett.* **2015**, *6*, 3082−3090.
(19) Ponseca, C. S., Jr.; Savenije, T. J.; Abdellah, M.; Zheng, K.; Yartsev, A.; Pascher, T.; Harlang, T.; Chabera, P.; Pullerits, T.; Stepanov, A.; Wolf, J.-P.; Sundström, V. Organometal Halide Perovskite Solar Cell Materials Rationalized: Ultrafast Charge Generation, High and Microsecond-Long Balanced Mobilities, and Slow Recombination. *J. Am. Chem. Soc.* **2014**, *136*, 5189−5192.
(20) Menke, S. M.; Holmes, R. J. Exciton Diffusion in Organic Photovoltaic Cells. *Energy Environ. Sci.* **2014**, *7*, 499−512.
(21) Kirchartz, T.; Mattheis, J.; Rau, U. Detailed Balance Theory of Excitonic and Bulk Heterojunction Solar Cells. *Phys. Rev. B: Condens. Matter Mater. Phys.* **2008**, *78*, 235320.
(22) Deschler, F.; Price, M.; Pathak, S.; Klintberg, L. E.; Jarausch, D.-D.; Higler, R.; Hüttner, S.; Leijtens, T.; Stranks, S. D.; Snaith, H. J.; Atatüre, M.; Phillips, R. T.; Friend, R. H. High Photoluminescence Efficiency and Optically Pumped Lasing in Solution-Processed Mixed Halide Perovskite Semiconductors. *J. Phys. Chem. Lett.* **2014**, *5*, 1421−1426.
(23) Yamada, Y.; Nakamura, T.; Endo, M.; Wakamiya, A.; Kanemitsu, Y. Photocarrier Recombination Dynamics in Perovskite $CH_3NH_3PbI_3$ for Solar Cell Application. *J. Am. Chem. Soc.* **2014**, *136*, 11610−11613.
(24) Narra, S.; Chung, C.-C.; Diau, E. W.-G.; Shigeto, S. Simultaneous Observation of an Intraband Transition and Distinct Transient Species in the Infrared Region for Perovskite Solar Cells. *J. Phys. Chem. Lett.* **2016**, *7*, 2450−2455.
(25) Ohta, N. Electric Field Effects on Photochemical Dynamics in Solid Films. *Bull. Chem. Soc. Jpn.* **2002**, *75*, 1637−1655.
(26) Hsu, H.-Y.; Chiang, H.-C.; Hu, J.-Y.; Awasthi, K.; Mai, C.-L.; Yeh, C.-Y.; Ohta, N.; Diau, E. W.-G. Field-Induced Fluorescence Quenching and Enhancement of Porphyrin Sensitizers on TiO_2 Films and in PMMA Films. *J. Phys. Chem. C* **2013**, *117*, 24761−24766.
(27) Ohta, N.; Awasthi, K.; Okoshi, K.; Manseki, K.; Miura, H.; Inoue, Y.; Nakamura, K.; Kono, H.; Diau, E. W.-G. Stark Spectroscopy of Absorption and Emission of Indoline Sensitizers: A Correlation with the Performance of Photovoltaic Cells. *J. Phys. Chem. C* **2016**, *120*, 26206−26216.
(28) Leijtens, T.; Kandada, A. R. S.; Eperon, G. E.; Grancini, G.; D'Innocenzo, V.; Ball, J. M.; Stranks, S. D.; Snaith, H. J.; Petrozza, A. Modulating the Electron-Hole Interaction in a Hybrid Lead Halide Perovskite with an Electric Filed. *J. Am. Chem. Soc.* **2015**, *137*, 15451−15459.
(29) Qiu, C.; Grey, J. K. Modulating Charge Recommbination and Structural Dynamics in Isolated Organometal Halide Perovskite Crystals by External Electric Fields. *J. Phys. Chem. Lett.* **2015**, *6*, 4560−4565.
(30) Xiao, Z.; Yuan, Y.; Shao, Y.; Wang, Q.; Dong, Q.; Bi, C.; Sharma, P.; Gruverman, A.; Huang, J. Giant Switchable Photovoltaic Effects in Organometal Trihalide Perovskite Devices. *Nat. Mater.* **2014**, *14*, 193−198.
(31) Umeuchi, S.; Nishimura, Y.; Yamazaki, I.; Murakami, H.; Yamashita, M.; Ohta, N. Electric Field Effects on Absorption and Fluorescence Spectra of Pyrene Doped in a PMMA Polymer Film. *Thin Solid Films* **1997**, *311*, 239−245.
(32) Tsushima, M.; Ushizaka, T.; Ohta, N. Time-Resolved Measurement System of Electrofluorescence Spectra. *Rev. Sci. Instrum.* **2004**, *75*, 479−485.
(33) De Quilettes, D. W.; Vorpahl, S. M.; Stranks, S. D.; Nagaoka, H.; Eperon, G. E.; Ziffer, M. E.; Snaith, H. J.; Ginger, D. S. Impact of Microstructure on Local Carrier Lifetime in Perovskite Solar Cells. *Science* **2015**, *348*, 683−686.
(34) Li, Y.; Yan, W.; Li, Y.; Wang, S.; Wang, W.; Bian, Z.; Xiao, L.; Gong, Q. Direct Observation of Long Electron-Hole Diffusion Distance in $CH_3NH_3PbI_3$ Perovskite Thin Film. *Sci. Rep.* **2015**, *5*, 14485.
(35) Wang, Q.; Shao, Y.; Xie, H.; Lyu, L.; Liu, X.; Gao, Y.; Huang, J. Quantifying Composition Dependent *p* and *n* Self-Doping in $CH_3NH_3PbI_3$. *Appl. Phys. Lett.* **2014**, *105*, 163508.
(36) Alemu, G.; Li, J.; Cui, J.; Xu, X.; Zhang, B.; Cao, K.; Shen, Y.; Cheng, Y.; Wang, M. Investigation on Regeneration Kinetics at Perovskite/oxide Interface with Scanning Electrochemical Microscopy. *J. Mater. Chem. A* **2015**, *3*, 9216−9222.
(37) Wu, C.; Li, F.; Guo, T. Efficient Tristable Resistive Memory Based on Single Layer Graphene/Insulating Polymer Multi-Stacking Layer. *Appl. Phys. Lett.* **2014**, *104*, 183105.
(38) Wetzelaer, G.-J. A. H.; Scheepers, M.; Sempere, A. M.; Momblona, C.; Avila, J.; Bolink, H. J. Trap-Assisted Non-Recombination in Organic-Inorganic Perovskite Solar Cells. *Adv. Mater.* **2015**, *27*, 1837−1841.
(39) Deretzis, I.; Alberti, A.; Pellegrino, G.; Smecca, E.; Giannazzo, F.; Sakai, N.; Miyasaka, T.; La Magna, A. Atomistic Origins of $CH_3NH_3PbI_3$ Degradation to PbI_2 in Vacuum. *Appl. Phys. Lett.* **2015**, *106*, 131904.
(40) Leguy, A. M. A.; Frost, J. M.; McMahon, A. P.; Sakai, V. G.; Kockelmann, W.; Law, C.; Li, X.; Foglia, F.; Walsh, A.; O'Regan, B. C.; Nelson, J.; Cabral, J. T.; Barnes, P. R. F. The Dynamics of Methylammonium Ions in Hybrid Organic-Inorganic Perovskite Solar Cell. *Nat. Commun.* **2015**, *6*, 7124.
(41) Leijtens, T.; Hoke, E. T.; Grancini, G.; Slotcavage, D. J.; Eperon, G. E.; Ball, J. M.; De Bastiani, M.; Bowring, A. R.; Martino, N.; Wojciechowski, K.; McGehee, M. D.; Snaith, H. J.; Petrozza, A. Mapping Electric Field-Induced Switchable Poling and Structural Degradation in Hybrid Lead Halide Perovskite Thin Films. *Adv. Energy Mater.* **2015**, *5*, 1500962.
(42) Bae, S.; Kim, S.; Lee, S.-W.; Cho, K. J.; Park, S.; Lee, S.; Kang, Y.; Lee, H.-S.; Kim, D. Electric-Field-Induced Degradation of Methylammonium Lead Iodide Perovskite Solar Cells. *J. Phys. Chem. Lett.* **2016**, *7*, 3091−3096.

DOI: 10.1021/acs.jpcc.7b07883
J. Phys. Chem. C 2017, 121, 22700−22706